Selection of mammalian cells based on their cell-cycle phase using dielectrophoresis

Unyoung Kim*, Chih-Wen Shu†, Karen Y. Dane‡, Patrick S. Daugherty‡, Jean Y. J. Wang†, and H. T. Soh*§¶

Departments of *Mechanical Engineering, ‡Chemical Engineering, and §Materials, University of California, Santa Barbara, CA 93106; and †Department of Medicine and Moores Cancer Center, School of Medicine, University of California at San Diego, La Jolla, CA 92093

Communicated by Alan J. Heeger, University of California, Santa Barbara, CA, September 18, 2007 (received for review May 11, 2007)

An effective, noninvasive means of selecting cells based on their phase within the cell cycle is an important capability for biological research. Current methods of producing synchronous cell populations, however, tend to disrupt the natural physiology of the cell or suffer from low synchronization yields. In this work, we report a microfluidic device that utilizes the dielectrophoresis phenomenon to synchronize cells by exploiting the relationship between the cell's volume and its phase in the cell cycle. The dielectrophoresis activated cell synchronizer (DACSync) device accepts an asynchronous mixture of cells at the inlet, fractionates the cell populations according to the cell-cycle phase (G_1/S and G_2/M), and elutes them through different outlets. The device is gentle and efficient; it utilizes electric fields that are 1–2 orders of magnitude below those used in electroporation and enriches asynchronous tumor cells in the G_1 phase to 96% in one round of sorting, in a continuous flow manner at a throughput of 2×10^5 cells per hour per microchannel. This work illustrates the feasibility of using laminar flow and electrokinetic forces for the efficient, noninvasive separation of living cells.

cell synchronization | microfluidics | cell sorting | electrokinetics

The cell cycle is comprised of a series of carefully coordinated cellular events encompassing the cell growth, the duplication of DNA, and the formation of daughter cells (1–3). Gentle and effective methods for synchronizing cells at a particular phase within the cell cycle are of significant biotechnological utility. For example, many anticancer drugs target cells in a particular phase [e.g., Paclitaxel targets the M phase by inhibiting microtubule disassembly (4), and Methotrexate targets the S phase by inhibiting dihydrofolate reductase (5)]; therefore, achieving effective synchrony of the tumor cell samples is critical to understanding their behavior and their response to chemotherapeutics.

Currently, there are two prevalent methods for achieving cell synchrony. The more widely used is the cell arrest and release technique (6), in which metabolic agents are used to arrest cells at a particular phase, allow other cells to accumulate at that phase, and then release them in synchrony by using a second chemical agent. Unfortunately, however, although this technique yields relatively high levels of synchrony, it has the undesirable effect of disturbing the normal physiology of the cell. In severe cases, the metabolic agents induce apoptosis (7, 8). The centrifugal elutriation technique (9) separates cells by injecting them into an elutriation rotor spinning at a constant *g*-force. When the centrifugal force is balanced with the opposing force from the flow rate, cells float and elute at specific positions. Although this method has some advantages over the cell arrest and release technique, it typically involves complex, time-consuming preparations and imposes significant mechanical stress on the cells (10). It thus appears that there is a need for facile, noninvasive methods for sorting cell populations according to their cell-cycle phase.

To address this need, we present a dielectrophoretic means (11) of selecting cells in a microfluidic device. The dielectrophoresis activated cell synchronizer (DACSync) device (Fig. 1*a*) fractionates the cells by exploiting the relationship between a mammalian cell's volume and its phase in the cell cycle (12) (i.e., a newly born cells in G_1 phase are the smallest and those in G_2 phase before mitosis are the largest). In this report, we describe the physics, modeling, and fabrication of the DACSync device, and demonstrate the dielectrophoretic enrichment of asynchronous tumor cells in G_1 phase to 96% synchrony.

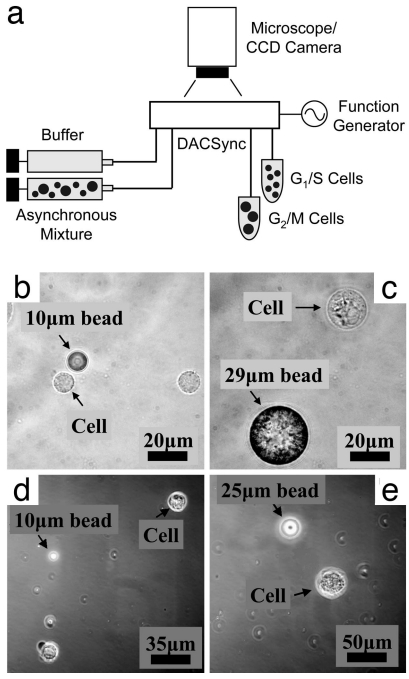

Fig. 1. Experimental setup of the DACSync device. (*a*) the DACSync chip is placed beneath an epifluorescence microscope, and the electrodes that power the dielectrophoresis (DEP) deflectors are connected to the function generator through two card-edge connectors. The frequency and magnitude of the applied voltage is measured through a digital oscilloscope. Two dual-track programmable syringe pumps deliver the sample mixture and buffer fluid. The flow pattern during the separation is monitored by a high-speed charge-coupled device (CCD) camera, and the eluted fractions from the two outlets are collected separately. (*b*) Optical micrograph of cells in G_1 phase with a 10-μm-diameter bead as a reference in size. (*c*) Cell in G_2/M phase with a 29-μm-diameter reference bead. (*d*) Cell arrested in G_1 phase by serum starvation with a 10-μm-diameter reference bead. (*e*) Cell arrested in G_1 phase by Lovastatin with a 25-μm-diameter reference bead.

Results and Discussion

Cell-Cycle Phase and Cell Size. The mammalian cell cycle consists of four distinct phases that differ by cell volume. In the G_1 gap

Author contributions: U.K., J.Y.J.W., and H.T.S. designed research; U.K. performed research; C.-W.S., K.Y.D., and P.S.D. contributed new reagents/analytic tools; U.K., C.-W.S., K.Y.D., J.Y.J.W., and H.T.S. analyzed data; and U.K. and H.T.S. wrote the paper.

The authors declare no conflict of interest.

¶To whom correspondence should be addressed. E-mail: tsoh@engineering.ucsb.edu.

www.pnas.org/cgi/doi/10.1073/pnas.0708760104

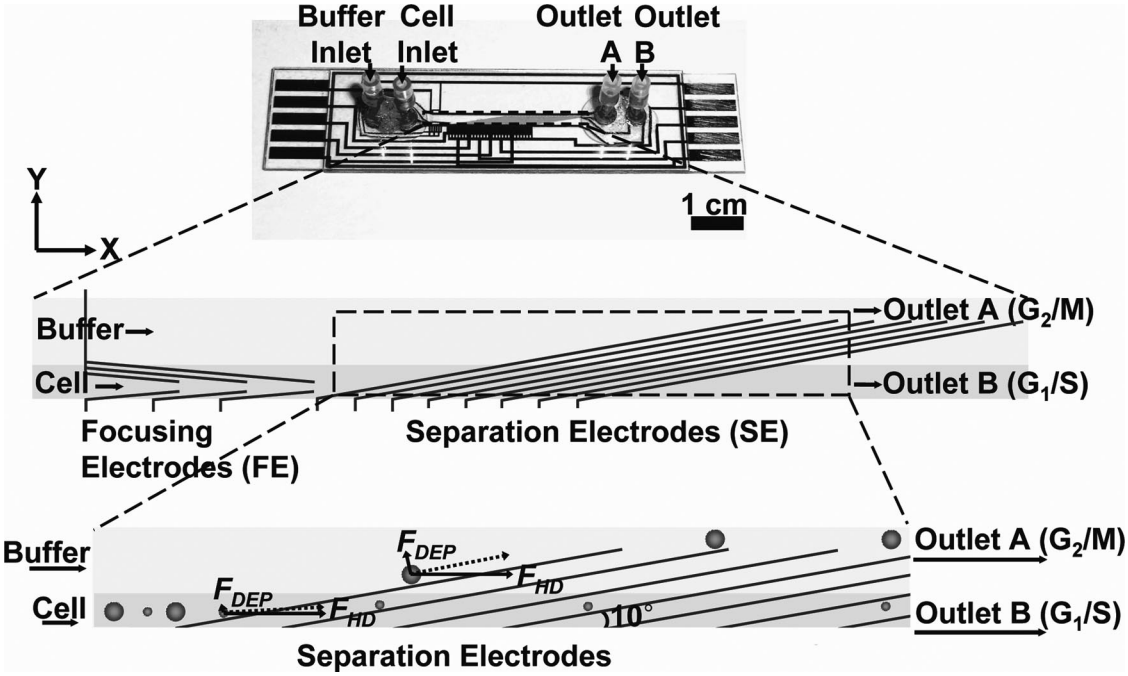

Fig. 2. The physics of separation for cells in difference phases in their cell cycle. Within the DACSync device there are two sets of electrodes: the focusing electrodes (FE) and the separation electrodes (SE). The FE ensure that the velocities of all particles are uniform before they enter the fractionation area, whereas the SE serve to separate the cells according to their phase in the cell cycle. For smaller G_1/S cells, the magnitudes of both the dielectrophoretic and hydrodynamic drag forces are less than those in the larger G_2/M phase. However, because the DEP force has a cubic dependence on cell size, whereas the hydrodynamic drag force has a linear dependence, the larger (G_2/M) cells experience a higher deflection force in the *Y* direction compared with the smaller (G_1/S) cells, thereby separating the two populations.

phase, the newly derived daughter cell undergoes metabolic expansion in preparation for DNA replication, which occurs during the synthesis (S) phase. The completion of DNA duplication in the S phase is followed by a second gap phase (G_2) during which the integrity of the replicated DNA is scrutinized to prepare for cell division. During mitosis (M), the DNA is condensed into chromatids, which align and segregate before the generation of two new daughter cells in the G_1 phase. The cell cycle is directional, irreversible, and almost universally correlated to cell size (12). Of note, this relationship between cell volume and the cell cycle holds true for bacteria (13), molds (14), and algae (15), as well as mammalian cells (16–23). Consistent with this fact, we have used bright-field microscopy to confirm that the volume of human breast ductal carcinoma cells used in this study (MDA-MB-231) undergo significant, concerted changes in cell volume during cell cycle; G_1/S cells have an average diameter of ≈10 μm (Fig. 1*b*) and increase to an average diameter of 20 μm during the G_2/M phase (Fig. 1*c*). Furthermore, to illustrate the point that the metabolic manipulation perturbs the cell's normal physiology, we have synchronized our cell line through serum starvation and two other commonly used metabolic agents (Lovastatin and Nocodazole) in G_1 and G_2 phases. Cells in G_1 phase synchronized by serum starvation are ≈18 μm in diameter (Fig. 1*d*), which is significantly larger than unperturbed cells. The perturbation is even greater for Lovastatin-arrested cells in G_1 phase (Fig. 1*e*), which are 35 μm in diameter. We also observed that the size of the cells in G_2/M phase arrested by Nocodazole is smaller than the cells in G_1 arrested by Lovastatin (data not shown). Thus, it is clear that the metabolic manipulation indeed has an effect on the cell's physiology; however, the extent of the perturbation is not clearly understood.

DACSync Device Design. There are two sets of electrodes within the DACSync device that serve separate functions (Fig. 2). The first set is the focusing electrodes (FE), which are designed at a glancing angle of 5° with respect to the flow, such that all incoming cells are deflected to the same *Y* position within the microchannel. This ensures that the velocities of all particles are uniform before they enter the separation area. The second set is the separation electrodes (SE), which separate the particles according to their volume. At every encounter with an electrode, the larger (G_2/M) cells experience a larger deflection force in the *Y* direction compared with the smaller (G_1/S) cells (Fig. 2, bottom). Thus, after passing through a set of SE, the G_2/M cells exit the device through outlet A, whereas G_1/S cells exit through outlet B. The SE are designed at an angle of 10° with respect to the flow.

Both FE and SE use the angled DEP electrode geometry, which has been previously implemented by a number of groups including ours (24–27). In this scheme, the electrodes operate in the negative DEP regime where the cells are physically repelled from areas of higher electric field gradients (i.e., near the electrode edges) into weaker field regions. This mode of operation is chosen because it minimizes the exposure of the cells to the electric fields. Quantitatively, the negative DEP force from the electrodes exerted on a spherical particle with a radius of *a* is approximately (28)

$$F_{\mathrm{DEP}} = \frac{27}{32}\,\pi^2 \varepsilon_{\mathrm{m}} \left(\frac{a}{h}\right)^3 \mathrm{Re}(CM) V^2, \qquad [1]$$

where ε_{m} is the permittivity of the suspension medium, *h* is the channel depth, *CM* is the Clausius–Mossotti factor (24, 25), and *V* is the rms magnitude of applied voltage. Concurrently, the particles also experience a hydrodynamic viscous drag force determined by Stokes's law:

$$F_{\mathrm{HD}} = 6\pi\mu v a, \qquad [2]$$

where μ is the viscosity of the fluid, and v is the velocity of the fluid. As the cells pass through the SE area, they experience the vector sum of the DEP force as well as the hydrodynamic force. However, because the F_{DEP} force has a cubic dependence on the radius, whereas the F_{HD} has a linear dependence, the ratio of the F_{DEP}/F_{HD} forces increases nonlinearly as a function of increasing radius. In other words, the larger (G_2/M) cells experience a higher deflection force in the Y direction compared with the smaller (G_1/S) cells, which gives rise to a nonuniform spatial concentration of cells in different phases (Fig. 2, bottom).

The spatial concentration distribution of cells in G_1/S and G_2/M phases through the device is calculated numerically by considering the DEP-modified velocities of the cells. The simulation code is written with the assumptions that each cell is spherical in shape and that, at the steady state, $\vec{F}_{DEP}$ and $\vec{F}_{DRAG}$ are balanced. $\vec{F}_{DRAG}$ is the component of $\vec{F}_{HD}$ in the opposite direction of $\vec{F}_{DEP}$. In this case,

$$0 = \vec{F}_{DEP} + \vec{F}_{DRAG}, \quad [3]$$

where the drag force ($\vec{F}_{DRAG}$) is given by the Stokes equation,

$$\vec{F}_{DRAG} = 6\pi\mu a(\vec{v}_p - \vec{v}). \quad [4]$$

The fluid velocity, $\vec{v}$, is obtained from solving the Navier–Stokes equation for a given geometry, and $\vec{v}_p$ is the DEP-modified particle velocity. Therefore, the DEP-modified particle velocity can be expressed as

$$\vec{v}_p = \frac{\vec{F}_{DEP}}{6\pi\mu a} + \vec{v}. \quad [5]$$

Once $\vec{v}_p$ is calculated, the concentration profile of the particles is obtained by using the Convection–Diffusion equation,

$$\frac{\partial C}{\partial t} + \nabla\cdot(\vec{v}_p C) = D\nabla^2 C, \quad [6]$$

where C is particle concentration, and D is the diffusion coefficient that can be approximated by the Stokes–Einstein equation. The resulting concentration profiles for larger G_2/M cells ($d = 2a = 20$ μm, where d is the diameter of the cells) and smaller G_1/S cells ($d = 10$ μm) are shown in Fig. 3 (*a* and *b*, respectively). It is clear that the populations of cells in different phases can be effectively separated during the encounter with the set of SE deflectors such that the G_2/M cells exit through outlet A, whereas the G_1/S cells exit through outlet B. A cross-section of the concentration profile at the two outlets confirms that almost all of the smaller cells will flow into outlet B (Fig. 3*c*).

There are several design parameters that are studied to optimize the cell synchronization performance. For example, from Eq. **1**, the F_{DEP} is proportional to $(a/h)^3$, whereas F_{HD} is linearly proportional to a. Thus, increasing the (a/h) ratio would provide a higher separation force, which would increase the throughput (i.e., number of cells processed per second per channel width) of the device. However, this design parameter must be considered in light of the practical fact that devices with larger (a/h) ratios have a much higher probability of clogging. Experimentally, we have found that a channel height of >40 μm allows continuous (>10 h) operation without fouling for the MDA-MB-231 tumor cells, whose diameters vary between 10 and 20 μm. Final design of the channel measures 1,400 μm in width, 2 cm in length, and 40 μm in height.

Furthermore, F_{DEP} is also proportional to the square of the applied voltage (V^2). Thus, an increase in the applied voltage would provide a significant increase in the separation efficiency and throughput; however, there are several practical considerations. The first limitation is cell viability; we measured the effect of electric fields on cell viability by performing an independent experiment on mouse B cells using Trypan blue staining in the DACSync device under typical operating conditions where the cells are exposed to the electric field for approximately a few seconds within the microchannel driven by an external source of 20-V peak-to-peak voltage at 800 Hz. We found that the difference in the percentage of viable cells before and after the DACSync processing was negligible using this assay. The high viability of the cells can be attributed to the fact that the DACSync device utilizes electric field strengths that are ≈1–2 orders of magnitude lower that those commonly used in electroporation (29). Furthermore, the fact that we operate the device in the negative DEP mode, such that the cells are being repelled away from the areas of high electric fields, may play a beneficial role.

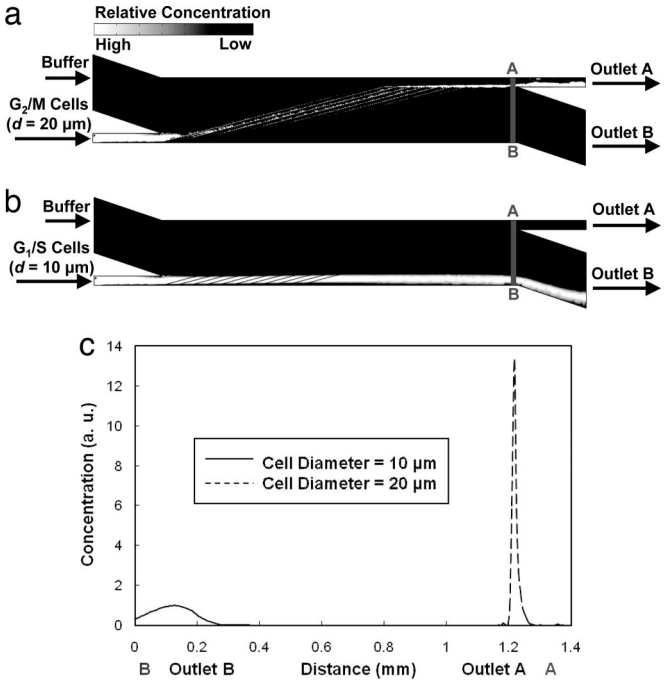

Fig. 3. Simulated concentration profiles of the cells in two different phases. (*a*) The larger cells in G_2/M phase undergo a larger deflection in the Y direction and subsequently exit through outlet A. (*b*) On the other hand, the smaller cells in G_1/S phase exit through outlet B. (*c*) Relative concentration profile of the cells in both phases along the A–B cross-section.

The second consideration on the operating voltage arises from the fact that higher electric fields induce electrolysis within the buffer due to the faradaic reactions at the electrodes. In our system which uses Au electrodes with buffer conductivity between 100 and 200 mS/m, we apply 20-V peak-to-peak voltage at 500 or 800 Hz for extended periods of time (>10 h) without electrolysis. Others have found that electrolysis may be further suppressed by optimizing buffer conditions (30) and electrode materials (31). We have also found that degassing the buffer solution before sorting is useful in inhibiting electrolysis.

Device Performance. The separation performance of the device was first characterized with a binary mixture of polystyrene beads (PSB). The initial PSB mixture contained 53% ($d = 2$ μm) and 47% ($d = 5$ μm) as measured by flow cytometry (Fig. 4*a*). Then, the mixture was sorted through the DACSync device at a throughput of $\approx 6 \times 10^5$ beads per hour per microchannel, and the PSB samples exiting through outlets A and B were collected separately and analyzed. Although some PSB are lost in the tubing and other fluidic interconnects, all beads that entered the

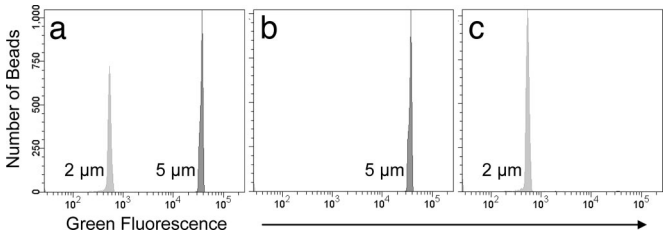

Fig. 4. Size-based separation of beads in the DACSync device measured by flow cytometry. DACSync is characterized with beads of two different sizes. The 5-μm-diameter beads are highly fluorescent (λ = 530 nm) compared with the 2-μm beads at the same wavelength. (*a*) Initial population consists of 47% 5-μm beads and 53% 2-μm beads. (*b*) The population of beads collected at outlet A consists of 99.97% 5-μm beads and 0.03% 2-μm beads, demonstrating a highly selective enrichment of the larger beads and depletion of the smaller beads. (*c*) The population of beads collected from outlet B consists of 0.08% 5-μm beads and 99.92% 2-μm beads, showing equally efficient enrichment of smaller beads.

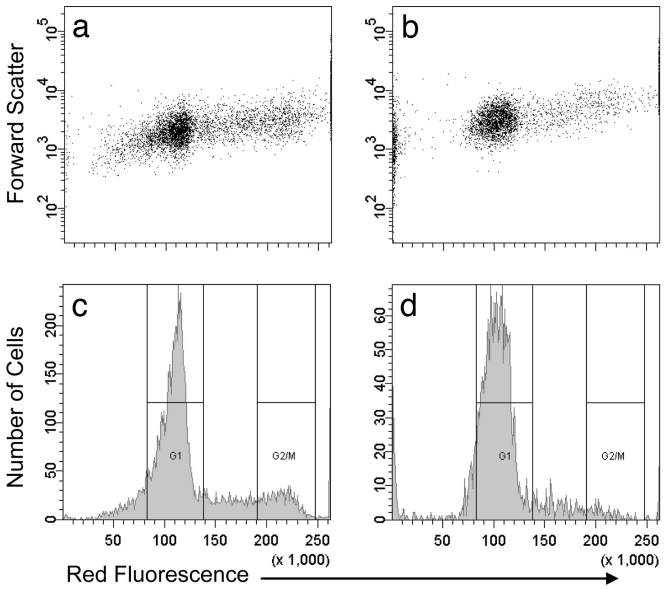

Fig. 5. The cell synchronization performance of the DACSync device measured by flow cytometry. Cell size (forward scatter) is measured as a function of the DNA content (PI, λ = 576 nm). (*a*) For the initial asynchronous mixture of cells, the positive slope of the distribution verifies the correlation between cell size and cell-cycle phase. (*b*) After one round of DACSync separation, the population of cells at outlet B demonstrates a significant increase in the population with low DNA content indicating a selective enrichment of cells in G_1 phase. (*c*) Histogram of the DNA content is used to verify this result. The initial asynchronous mixture has a G_1:G_2/M ratio of 5.2:1. (*d*) After the DACSync sorting, the measured G_1:G_2/M ratio for the population of cells from outlet B is 23:1.

device were successfully recovered and no bead-sticking in the device was observed through the charge-coupled device (CCD) camera (data not shown). The device shows exceptional volume-based separation; the fraction eluted through outlet A were dominantly 5-μm beads (99.97%), and only 0.03% were the smaller, 2-μm beads (Fig. 4*b*). In contrast, fraction eluted through outlet B primarily consisted of 2-μm beads (99.92%), and only 0.08% were the larger, 5-μm beads (Fig. 4*c*).

The synchronization performance of the MDA-MB-231 human breast tumor cells was measured such that the smaller (G_1) cells were enriched through outlet B. We have chosen this configuration because the cells reside in G_1/S phase for a much longer period than in G_2/M phase [typically 16–24 h in G_1/S phase compared with 2.5–3 h in G_2/M phase (32)]. Thus, the probability of the G_1/S phase entering the G_2/M phase during the experiment is significantly less than the probability of cells in the M phase dividing and giving rises to two G_1 cells, which would result in undesired degradation in purity. After the cells are harvested from culture, the mixture of cells is suspended in the sorting buffer and injected into the DACSync device at a throughput of $\approx 2 \times 10^5$ cells per hour per microchannel. The separation electrodes are powered at 20 V peak-to-peak and 800 kHz. After the synchronization, the cells were fixed in the collection tubes, which were prefilled with chilled ethanol. The propidium iodide (PI) staining method (33) with flow cytometry is used for quantitative determination of the cell-cycle phase; because PI is a DNA intercalating dye, the fluorescence intensity is directly proportional to the DNA content and, thus, the cell-cycle phase. We found that the size of the cells [forward scatter (FSC)] is positively correlated with DNA content (red fluorescence) for the initial mixture (Fig. 5*a*) as well as synchronized cells (Fig. 5*b*), which confirms the fact that the cell size and its phase in the cell cycle are indeed correlated. Furthermore, the decrease in population with high FSC and red fluorescence after sorting verifies that cells in G_2/M phase are successfully depleted at outlet B. More quantitatively, we compared the histograms of red fluorescence, before and after the DACSync processing. In the initial asynchronous mixture, the ratio of the cells in G_1 phase to those in G_2/M phase is $\approx$5.2:1 (Fig. 5*c*), which is approximately consistent with the relative duration of the G_1 phase compared with the G_2/M phase. In contrast, after a single pass through the device, the ratio of G_1 to G_2/M cells increased to 23:1 (Fig. 5*d*) and the cell synchrony in the G_1 phase (i.e., the fraction of cells in the target phase) reached 96%.

Conclusion. We demonstrate the use of the dielectrophoresis phenomenon to select mammalian cells according to the phase in their cell cycle. The DACSync device offers the capability to purify and enrich cells in a particular phase from an asynchronous mixture in a continuous-flow manner. The method uses electric field strengths that are significantly lower than those commonly used for electroporation, and combined with the fact that the device operates in a mode where the cells are repelled away from the areas of high electric fields (i.e., negative DEP), we found that the method can be gentle and have minimal effect on the cell viability. Currently, the processing throughput of DACSync is limited to $\approx 10^5$ cells per hour per microchannel; however, it may be possible to integrate multiple channels to increase the processing capacity. Finally, by implementing a device architecture with variable electrode angles and multiple outlets, it may be possible to sort an asynchronous mixture into multiple subpopulations within a particular phase.

Materials and Methods

Bead Samples and Buffer Conditions. Red (diameter = 2 μm) and green (diameter = 5 μm) fluorescent polystyrene beads were purchased from Duke Scientific and used at the concentrations of 0.53×10^6 beads per ml and 0.47×10^6 beads per ml, respectively. The bead mixture was suspended in 0.1$\times$ PBS supplemented with 1% BSA (Fraction V; Sigma–Aldrich) to prevent agglomeration and adsorption of the particles on the electrodes of the DACSync device. To prevent settling of the beads during fractionation, the density of solution was adjusted to that of polystyrene beads (1.06 g/ml) with glycerol at a final concentration of 20% (vol/vol).

Cell Line and Culturing and Buffer Conditions. Human breast ductal carcinoma cell line (MDA-MB-231) was used in this study. The cells were cultured in Dulbecco's modified Eagle's medium (DMEM) (Invitrogen) with 10% FBS (Invitrogen). To ensure normal growth conditions, asynchronous cells were harvested from a culture dish when it reached 70% confluency. The cells were pelleted and resuspended (1×10^6 cells per ml) in 0.1$\times$ PBS supplemented with 2% BSA (Fraction V; Sigma–Aldrich) and 1 mM EDTA (Sigma–Aldrich). Before

DACSync operation, the density of solution was adjusted with sucrose to a final concentration of 8.5% (vol/vol) to prevent the settling of the cells.

Synchronization of Cells by Cell Arrest and Release. To arrest the cells by serum starvation, the cells were cultured in DMEM without FBS for 32 h. For late G_1 arrest by Lovastatin, the cells were cultured in DMEM with 10% FBS with 50 μM Lovastatin for 32 h. For M arrest by Nocodazole, cells were culture in DMEM with 10% FBS with 0.2 μg/ml Nocodazole for 18 h. All arrested cells were fixed with ethanol on ice for 2 h before microscopic imaging.

Device Microfabrication. The DACSync device was fabricated in a manner similar to the dielectrophoresis activated cell sorter (DACS) devices described in our previous work (24). Briefly, top and bottom electrodes were patterned with 20 nm of titanium and 200 nm of gold on top of 4-inch glass wafers (Pyrex 7740 borosilicate glass; Corning) through e-beam evaporation (Temescal). Then, photosensitive polyimide (HD4010; HD MicroSystems) was spun on the top and bottom substrates at 1,500 rpm for 45 sec, which results in a 40-μm-thick film after curing and bonding. Microfluidic channels were defined on this layer by photolithography using standard exposure tools (SUSS; 350-nm wavelength, 1-min exposure), and the polyimide layer was subsequently developed (2 min in 100% developer, 2 min in 50% developer and 50% rinser, and 30 sec in 100% rinser). The polyimide layer served as the spacer between the two glass substrates. After drilling microfluidic vias on the top substrate with a computer-controlled milling machine (Flashcut CNC) and dicing both substrates, the two pieces were aligned and bonded at 300°C for 2 min by using a Flip-Chip aligner bonder (Research Devices). To complete the bonding process, a wafer bonder (SB-6; SUSS MicroTec) was used where the bonded device was placed in a nitrogen environment and the polyimide was cured at 375°C for 40 min and then bonded for 10 min. Microfluidic inlets and outlets were manually fixed on the drilled vias of the device using epoxy.

Numerical Simulations. Numerical simulations were performed to optimize the electro-hydrodynamic design. Commercially available finite element analysis software (Multiphysics 3.1; Comsol) was used. For a given design, the velocity profile was calculated by solving the ''Incompressible Navier–Stokes Mode.'' In the ''Subdomain Settings,'' viscous drag force was incorporated into volume force, and in the ''Boundary Settings,'' velocities at the inlets were set to have a parabolic profile, while the pressure at the outlets was set to zero. All other boundary conditions were set to have no-slip conditions. In the ''Convection and Diffusion Mode,'' the *X* and *Y* directional velocities from DEP forces were calculated in ''Scalar Expressions,'' and the final velocities were obtained by combining the velocities calculated from ''Navier–Stokes Mode'' and DEP force. A mesh size of <4 μm was used near deflecting electrodes to model the DEP force accurately.

Device Testing and Cytometry. During the sorting operation, the DACSync device was placed beneath the objective of an epifluorescence microscope equipped with charge-coupled device (CCD) camera (Hamamatsu), and the DEP electrodes were connected to the function generator (AFG320; Tektronix) through two card-edge connectors. The frequency and magnitude of the applied voltage were measured with a digital oscilloscope (54622A; Agilent Technologies). Two dual-track programmable syringe pumps (PhD 2000; Harvard Apparatus) deliver the mixture and the buffer fluid with a combined flow rate of 200–400 μl/h. When the flow pattern was stabilized, a sine wave of 20 V peak-to-peak at 500 kHz (for bead fractionation) or 800 kHz (for cell synchronization) was applied to the set of electrodes. The two outlets of the DACSync device were collected separately in 1.5-ml centrifuge tubes. To fix the collected cells immediately after sorting, the centrifuge tubes were prefilled with ethanol on ice.

A fluorescence-activated cell sorter (FACSAria; BD Biosciences) was used to characterize the sorting performance for bead and cell samples. To quantify the degree of synchronization of cells, the two eluted fractions from two separate outlets were stained with PI ($\lambda = 576$ nm; Sigma–Aldrich) before the cytometric analysis using standard methods; the collected cells were first fixed in ethanol on ice for $\approx$2 h, pelleted, resuspended in 1$\times$ PBS, and stained with PI solution containing 1$\times$ PBS with 0.1% (vol/vol) Triton X-100 (Sigma–Aldrich). The stained cells were supplemented with RNase (Sigma–Aldrich) to 200 μg/ml final concentration, incubated for 20 min at room temperature, and analyzed with flow cytometry.

ACKNOWLEDGMENTS. We thank Dr. Xiaoyuan Hu and Prof. Carl D. Meinhart for helpful discussions and Prof. Kevin W. Plaxco for his careful reading of the manuscript. Microfabrication was carried out in the Nanofabrication Facility at the University of California, Santa Barbara. This work was supported by Beckman Young Investigator Program Grant 8-442550-57174, Army Research Office Institute for Collaborative Biotechnologies Grant DAAD1903D004, Defense Advanced Research Projects Agency/Defense Microelectronics Activity–Center for Nanoscale Innovation for Defense Grant H94003-05-2-0503, and University Education Partnership Program Grant 8-482550-26752 from the Livermore National Laboratories.

1. Lee MG, Nurse P (1987) *Nature* 327:31–35.
2. Hartwell LH, Weinert TA (1989) *Science* 246:629–634.
3. Evans T, Rosenthal ET, Youngblom J, Distel D, Hunt T (1983) *Cell* 33:389–396.
4. Schiff PB, Fant J, Horwitz SB (1979) *Nature* 277:665–667.
5. Jolivet J, Cowan KH, Curt GA, Clendeninn NJ, Chabner BA (1983) *N Engl J Med* 309:1094–1104.
6. Jackman J, O'Connor PM (1998) in *Current Protocols in Cell Biology*, eds Bonifacino JS, Dasso M, Harford JB, Lippincott-Schwartz J, Yamada KM (Wiley, New York), Chap 8.3.
7. Gong J, Traganos F, Darzynkiewicz Z (1995) *Cell Growth Differ* 6:1485–1493.
8. Schimke RT, Kung AL, Rush DF, Sherwood SW (1991) *Cold Spring Harbor Symp Quant Biol* 56:417–425.
9. Davis PK, Ho A, Dowdy SF (2001) *BioTechniques* 30:1322–1324.
10. Hohmann LK, Shows TB (1979) *Somatic Cell Mol Genet* 5:1013–1029.
11. Pohl HA (1978) *Dielectrophoresis: The Behavior of Neutral Matter in Nonuniform Electric Fields* (Cambridge Univ Press, Cambridge, UK).
12. Jorgensen P, Tyers M (2004) *Curr Biol* 14:1014–1027.
13. Donachie WD (1968) *Nature* 219:1077–1079.
14. Sachsenmaier W, Donges KH, Rupff H (1970) *Z Naturforsch* 25:866–871.
15. Donnan L, John PC (1983) *Nature* 304:630–633.
16. Killander D, Zetterberg A (1965) *Exp Cell Res* 38:272–284.
17. Killander D, Zetterberg A (1965) *Exp Cell Res* 40:12–20.
18. Dolznig H, Grebien F, Sauer T, Beug H, Mullner EW (2004) *Nat Cell Biol* 6:899–905.
19. Shields R, Brooks RF, Riddle PN, Capellaro DF, Delia D (1978) *Cell* 15:469–474.
20. Galavazi G, Bootsma D (1966) *Exp Cell Res* 41:438–451.
21. Stancel GM, Prescott DM, Liskay RM (1981) *Proc Natl Acad Sci USA* 78:6295–6298.
22. Kimball RF, Perdue SW, Chu EH, Ortiz JR (1971) *Exp Cell Res* 66:17–32.
23. Ramirez OT, Mutharasan R (1990) *Biotechnol Bioeng* 36:839–848.
24. Hu X, Bessette PH, Qian J, Meinhart CD, Daugherty PS, Soh HT (2005) *Proc Natl Acad Sci USA* 44:15757–15761.
25. Kralj JG, Lis MTW, Schmidt MA, Jensen KF (2006) *Anal Chem* 78:5019–5025.
26. Fiedler S, Shirley SG, Schnelle T, Fuhr G (1998) *Anal Chem* 70:1909–1915.
27. Seger U, Gawad S, Johann R, Bertsch A, Renaud P (2004) *Lab Chip* 4:148–151.
28. Gascoyne PRC, Vykoukal J (2002) *Electrophoresis* 23:1973–1983.
29. Fox MB, Esveld DC, Valero A, Luttge R, Mastwijk HC, Bartels PV, van den Berg A, Boom RM (2006) *Anal Bioanal Chem* 385:474–485.
30. Studer V, Pepin A, Chen Y, Ajdari A (2004) *Analyst* 129:944–949.
31. Xie J, Miao Y, Shih J, He Q, Liu J, Tai Y, Lee TD (2004) *Anal Chem* 76:3756–3763.
32. Lodish M, Berk A, Matsudaira P, Kaiser CA, Krieger M, Scott MP, Zipursky SL, Darnell J (2004) *Molecular Biology of the Cell* (Freeman, New York), 5th Ed.
33. Darzynkiewicz Z, Juan G, Bedner E (1999) in *Current Protocols in Cell Biology*, eds Bonifacino JS, Dasso M, Harford JB, Lippincott-Schwartz J, Yamada KM (Wiley, New York), Chap 8.4.